The Effect of Sintering Condition on the Properties and Transpiration Cooling Performance of Porous Ni-based Superalloy

Jukyoung Shin, Junhyeon Bae, Tae Young Kim*

Dept. of Mechanical and Automotive Eng. , Seoul National Univ. of Science and Technology

Abstract

The development of a Thermal Protection System (TPS) is crucial for reusable space vehicles to protect from extremely high temperatures during atmospheric re-entry, caused by air friction and shockwaves leading to adiabatic compression effects. Transpiration cooling involves the use of porous media, allowing the flowing fluid to absorb and evaporate heat, facilitating efficient heat transfer, which provides excellent cooling performance. In this study, porous metal was produced using a powder sintering process with nickel-based superalloy powder. To analyze the transpiration cooling performance depending on physical characteristics such as porosity, permeability, and pore size of the specimens, the physical property changes were examined based on the powder sintering process parameters, such as compaction pressure and sintering temperature. Subsequently, the transpiration cooling performance was evaluated.

Keywords: *Transpiration cooling, Phase change, Sintered porous metal, porosity, permeability, Reusable space vehicle*

1. Introduction

1.1. Background

With recent advancements in space vehicle technology, the New Space era, led by private companies, has emerged. Particularly, the development of reusable space vehicle technology has significantly reduced launch costs, leading to the discovery of various applications in space technology, including material transportation, satellite communication, and space tourism. However, during re-entry into the atmosphere, reused space vehicles are exposed to extreme thermal environments due to aerodynamic heating caused by air friction and adiabatic compression effects caused by shock waves, resulting in severe damage to the outer walls. Therefore, the design of a thermal protection system to protect space vehicles is very important, and previously, heat shields and ablative coatings using Ultra-High Temperature Ceramics (UHTC's) and Reinforced Carbon-Carbon (RCC) have been applied [1-4]. However, these material-based technologies require high maintenance costs and time to replace damaged protective materials after re-entry. Therefore, there is a growing need to implement active cooling technologies that can effectively cool space vehicles to ensure complete, maintenance-free reusability.

Active cooling structure technologies include convective, film, regenerative, and transpiration cooling [5]. Among these, transpiration cooling is a technology in which liquid coolant absorbs heat from surrounding structures as it penetrates a porous medium, undergoes a phase change to remove the heat, and is then discharged to the external surface to form a protective film that protects the structure. Transpiration cooling technology has uniform cooling performance because it uses porous media and has higher cooling efficiency than other active cooling structural technologies due to its high surface

---

area and phase change flow. Because of these advantages, transpiration cooling is being studied as a next-generation thermal protection system for reusable space vehicles [6-8].

1.2. Objectives

In this study, a diameter 60mm porous nickel-based superalloy was fabricated using the metal powder sintering method, and the feasibility of specimen production and the variation of physical properties were investigated based on various process parameters during the specimen fabrication process. To simulate the high-temperature environment occurring during re-entry, a gas torch was employed, and experiments were conducted with the torch and specimen arranged vertically to eliminate the influence of gravity on the radial direction of the specimen.

In transpiration cooling, the internal flow field of the porous specimen can be classified into liquid region, mixture region, and superheated vapor region, depending on the phase of the penetrating fluid, the interface positions between these three regions change according to the heat flux applied to the specimen and the coolant mass flow rate. When the heat flux is kept constant, a decrease in the coolant mass flow rate results in the occurrence of the liquid-mixture interface at the top of the specimen first. Subsequently, the liquid-mixture interface moves downward, and the mixture-vapor interface occurs at the top. As the coolant decreases further, the liquid region disappears, and eventually, the mixture region also disappears. Therefore, during the transpiration cooling process, five flow patterns may exist in the porous plate:

(1) All liquid: State where the coolant is in a liquid state, and only the liquid region exists within the medium as sufficient cooling has been achieved.

(2) liquid-mixture: State where the mixture region appears as the phase change begins from the heating surface, but the superheated vapor region is not present.

(3) liquid-mixture-vapor: State where the superheated vapor region appears from the heating surface, and all three regions of liquid, mixture, and vapor appear within the porous media.

(4) mixture-vapor: State where there is no liquid region within the porous media and only the mixture and superheated vapor regions are present.

(5) All vapor: State where the entire region within the porous media is superheated vapor.

The changes in the interface between these five flow patterns greatly affect the heat transfer and pressure characteristics of transpiration cooling. Due to the complexity of the phase change flow within the porous medium, analyzing the mechanism and performance of transpiration cooling is challenging. Therefore, in this study, we aim to observe the five flow patterns by reducing the amount of coolant under conditions of high heat flux occurring during space re-entry using directly fabricated porous specimens. Additionally, we intend to analyze the heat transfer and pressure characteristics according to the five flow patterns to propose a coolant mass flow rate that can minimize the weight of the coolant, which is closely related to launch costs.

2. Experiment

2.1.1 Specimen

In this study, the metal powder sintering method was employed to fabricate specimens suitable for use as the outer walls of space vehicles, capable of transpiration cooling. This method relies on the principle of metal powder being heated to temperatures below its melting point and then bonding through material diffusion, allowing for the uniform and mechanically robust fabrication of three-dimensional porous metal specimens. Nickel-based alloy Hastelloy X, renowned for its excellent resistance to oxidation, corrosion, and high temperatures, was chosen for the metal powder to withstand the extreme environments of space and the high temperatures encountered during atmospheric re-entry.
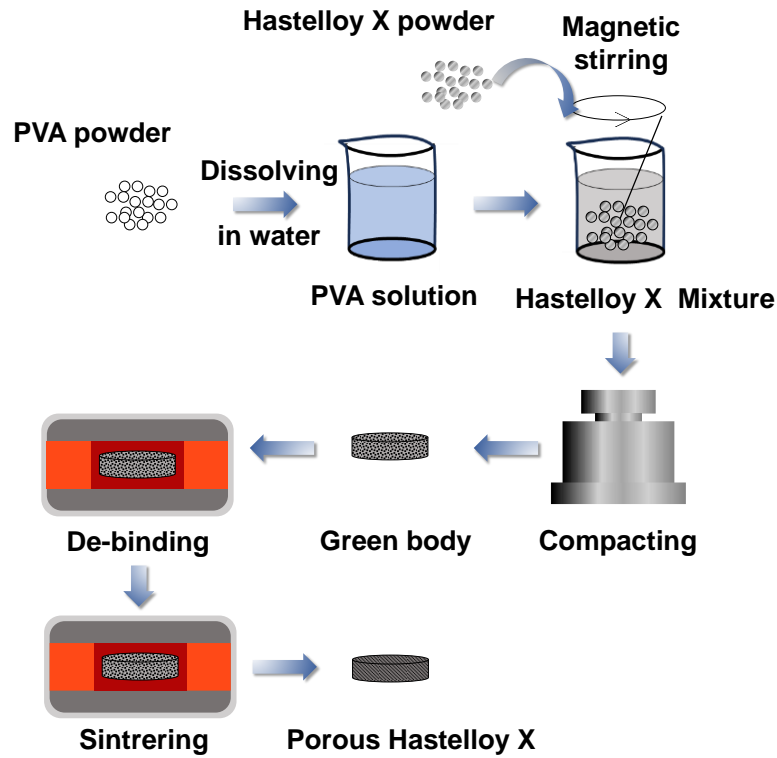
Fig. 1 Porous specimen fabrication process

Table 1.   Porous specimen fabrication variable

| Compacting pressure (kPa)	Sintering temperature (℃)	Sintering time (h)
100 - 300	1100 - 1200	2 - 4

As shown in Fig. 1, the metal powder sintering process consists of mixing, compacting, de-binding, and sintering stages. The mixing stage is divided into two processes: preparing the binder solution to hold the powder in place and mixing the binder solution with the metal powder to create a metal slurry. Polyvinyl alcohol (PVA) was used as the binder, and the metal powder and PVA solution were mixed for 30 minutes to ensure uniformity. Subsequently, in the forming stage, the metal slurry was shaped into disk-shaped green bodies using a hand-pressing machine under constant pressure for 30 minutes, taking into account the volume changes due to thermal deformation during sintering. Next, in the de-binding stage, the organic binder remaining in the green bodies was removed by heating them in a furnace to 600 ℃, the temperature at which PVA evaporates, and maintaining it for 3 hours. To prevent crack formation due to the expansion of PVA between the powder particles, the temperature was gradually increased at a rate of 3 ℃/min. Additionally, argon was injected at a rate of 3 L/min to prevent oxidation of the metal. After the de-binding step, the sintering process heats the green body at a rate of 5°C/min to near the melting point of the metal powder and holds it in the furnace for 2 hours. Sintering was conducted under the conditions listed in Table 1 to analyze the characteristics of the specimens concerning changes in compacting pressure, sintering temperature, and sintering time.

2.1.2 Experimental setup

As illustrated in Fig. 2, the experimental setup consists of a heating system, cooling system, test section, and measurement system. To simulate the extreme heat environment experienced during space re-entry, an oxygen-acetylene gas torch was utilized as the heating system. The torch was

The Effect of Sintering Condition on the Properties and Transpiration Cooling Performance of Porous Ni-based Superalloy

positioned vertically relative to the specimen, ensuring that the flame collided perpendicularly with the specimen. A torch nozzle was designed to uniformly heat a 60 mm heating area. Heat flux was measured based on the gas mass flow rate and the distance between the nozzle and the heating surface to analyze the transpiration cooling characteristics of porous specimens under constant heat flux conditions. The gas mass flow rate was controlled consistently using a mass flow controller (MFC Korea, MFC VIC-D220).

For the cooling system, a two-head high-pressure piston pump (FLOM, Intelligent SS) capable of delivering a full-scale flow rate of 1000 ml/min was employed to supply coolant. To analyze the effect of coolant flow rate on transpiration cooling performance and phase-change flow, a piston pump capable of supplying a constant flow rate of coolant was utilized. This pump employs two pistons connected to alternately perform drawing and injecting operations, ensuring the continuous supply of coolant at a constant flow rate without pulsations for an extended period. The coolant flow rate can be controlled by a computer program with an accuracy of ±0.5%FS.
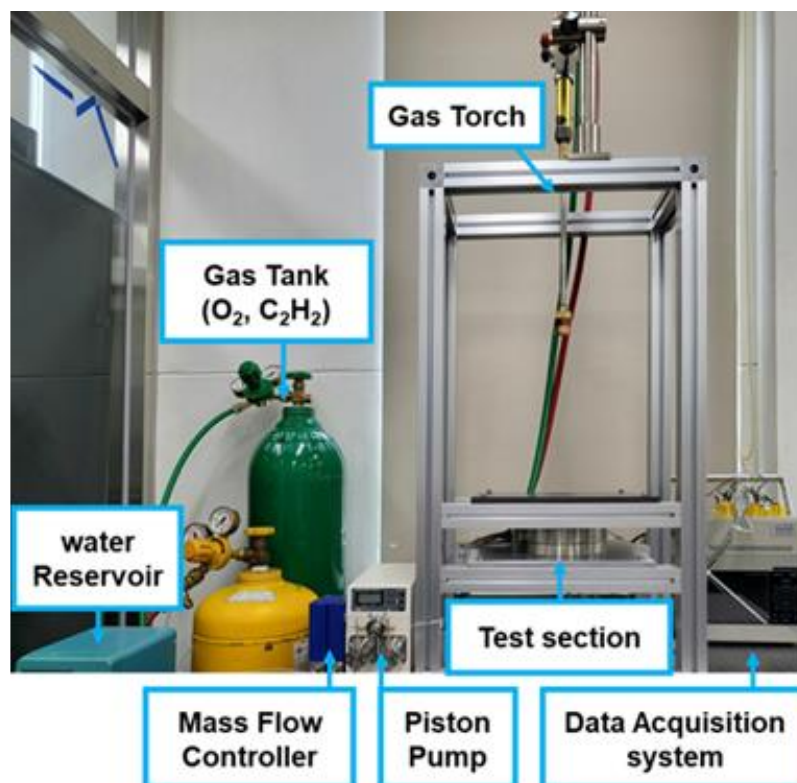
Fig. 2 Experimental setup

As shown in Figure 3, the test section consists of the porous specimen, upper housing, lower housing, and seal, as well as the temperature measurement points. The porous specimen was clamped between stainless steel upper and lower housings, and a graphite spiral gasket was used to prevent coolant leakage from the clamping surface under high temperature and pressure conditions. Coolant is injected into the coolant chamber through a pipe connected to the lower housing and is uniformly supplied to the bottom of the specimen, then passes through the specimen and is ejected to the top of the specimen, which is exposed by the upper housing to a diameter of 60 mm. temperature of the porous specimen was measured using an IR camera (FLUKE, Ti480 Pro) and a pyrometer, while the temperature at the bottom and side was measured using a K-type thermocouple. To estimate the system pressure, a pressure sensor (PSH, SENSYS) with an accuracy of ±0.15%FS was used.
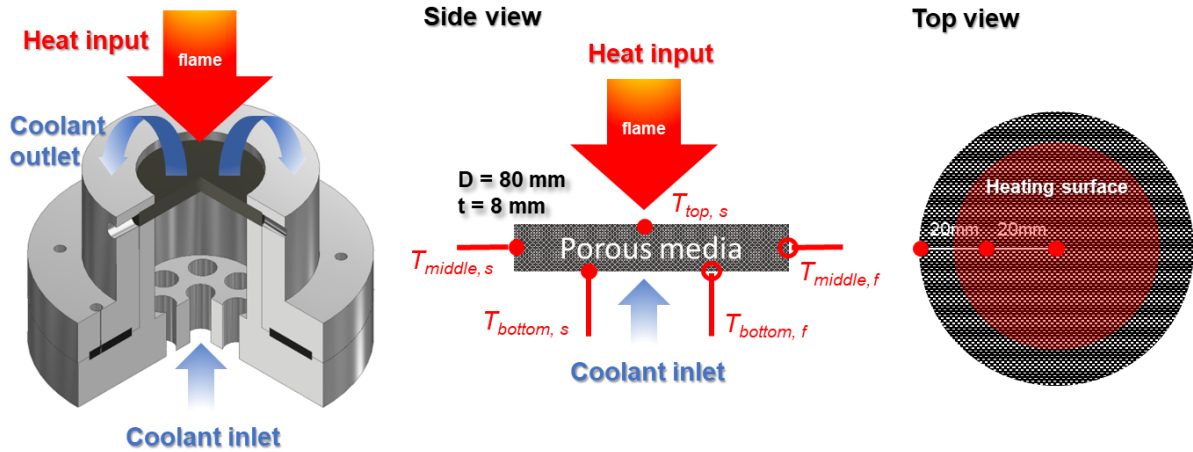
Fig. 3 Test section and temperature measurement point

2.1.3 Procedure

In this study, a heat flux of 0.22 MW/m2 was applied, and deionized water was injected into the specimen mass flow rate ranging from 0.13 to 0.26 g/s to observe flow characteristics and measure temperature and pressure. When the specimen was at room temperature, it took a significant amount of time to reach a steady state when both the heating and cooling systems were operated simultaneously, as the liquid coolant ejected onto the specimen heating surface and formed a liquid film. Therefore, the heating system was operated first, and the cooling system was activated when the temperature of the heating surface reached 100 ℃. Additionally, to prevent damage to the specimen due to high temperatures during initial heating, all initial specimens were filled with water. To analyze the heat transfer and pressure characteristics of transpiration cooling, the temperature variation of the heating surface of the specimen was considered stable when it remained below 0.1% for 5 minutes. Temperature and pressure data were then collected for 5 minutes, and the average was calculated. All measurements were conducted using a multifunctional measurement device with measurements taken at intervals of 0.5 seconds. The experiments were repeated by gradually reducing the mass flow rate of the coolant from the highest value to observe the specimen's response under constant heat flux conditions.

3.   Results and discussions

3.1.1 Effect of sintering conditions on the porous specimen

The formability based on the concentration and quantity of the PVA solution mixed with Hastelloy X was analyzed. As shown in Fig. 4, the specimens were fabricated with varying concentrations and quantities of PVA solution. When the concentration of the PVA solution was high, the viscosity of the metal powder slurry increased, making it difficult to separate from the compacting mold. Conversely, when the concentration was low, the formability of the metal powder slurry decreased. Moreover, a larger quantity of PVA solution resulted in longer drying times, while a smaller quantity led to inadequate mixing of the metal powder and binder. These findings indicate that the best formability was achieved when a 5 wt% concentration of PVA solution was mixed with the metal powder at a mass ratio of 5:100.

Fig. 4 Schematic diagram of the effect of PVA solution on metal slurry formability

In this study, specimens with a porosity of 0.3, fabricated under the conditions outlined in Table 2, were utilized. As depicted in Figure 5, the fabricated disk-shaped specimens with a diameter of 80 mm, along with microscopic images of the specimens. Upon observing the microscopic images of the specimens, it is evident that spherical Hastelloy X powder particles, each with a size of 50 µm, are bonded together to form necks, with pores formed in between, serving as cooling channels. The necks are structures formed by the bonding of metal powder particles under high pressure and high temperature during the fabrication process. The formation of necks is influenced by the compacting pressure, sintering temperature, and sintering time. Moreover, as the necks grow, the distance between the powder particles decreases, leading to a reduction in the size of the formed pores.
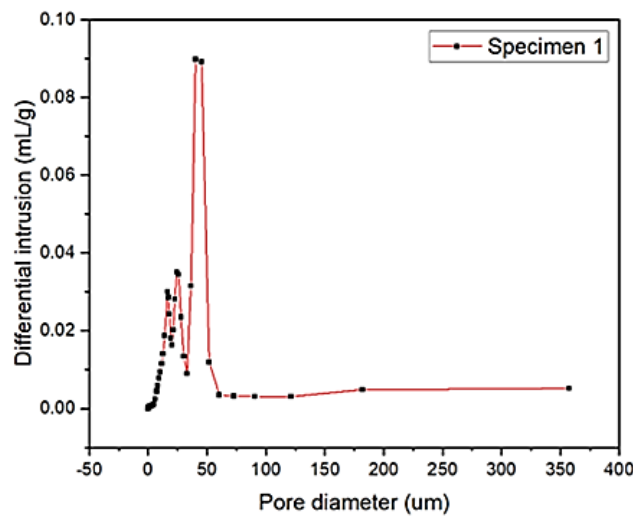
Table 2.   Sintering conditions

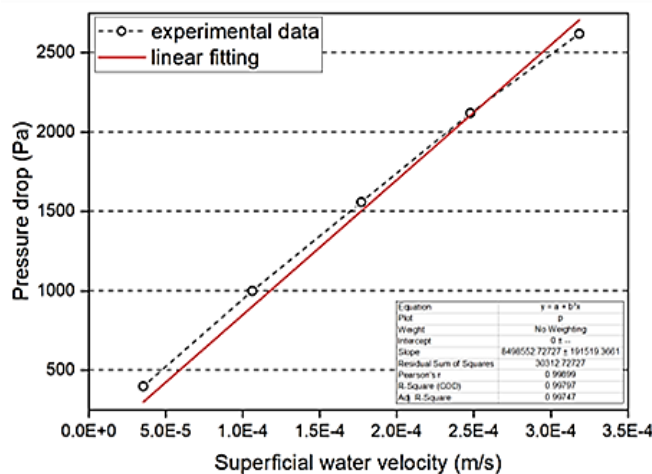| Compacting pressure (kPa)	Sintering temperature (℃)	Sintering time (h)
223	1100	2
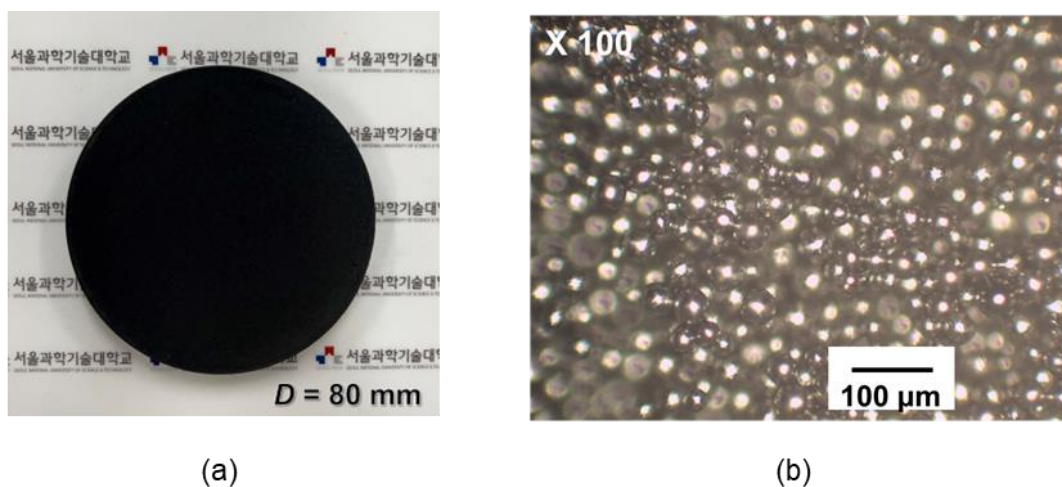
Fig. 5 (a) Specimen image, (b) microscopic image of the specimen

As presented in Fig. 6, the results of the pore-size distribution analysis and permeability measurement were conducted to verify the physical characteristics of the specimens. The porosity and pore diameter of the sintered specimens were measured using a pore-characterizing system (Micromeritics, AutoPore 9520), which injects mercury into the specimen under varying pressures to measure the existing porosity and pore diameter. From Figure 6 (a), it can be observed that the pore-size distribution, representing the size of channels for coolant in the transpiration cooling system, peaks at 48 − 50 μm. This indicates that the fabricated specimens form pores of uniform size.

To measure the permeability of the specimens, Darcy's equation, which relates the flow rate of coolant penetrating the porous medium to the pressure gradient, was utilized. As shown in Figure 6 (b), the graph of coolant flow rate versus pressure was measured when varying the coolant velocity injected into the specimen. By linearly fitting the data points, the slope obtained provides the calculated permeability of the specimen, which is 1e-14 m^2.


(a)

(b)

Fig. 6 (a) Differential instruction curve, (b) permeability measurement result

The Effect of Sintering Condition on the Properties and Transpiration Cooling Performance of Porous Ni-based Superalloy

3.1.2 Two-phase flow patterns

In this study, experiments were conducted by applying a heat flux of 0.22 MW/m2 to the top surface of porous Hastelloy X specimens with a porosity of 0.3, while varying the flow rate of 300 K cooling water in the range of 0.1 to 0.26 g/s. As a result, characteristics similar to the five flow patterns described earlier were observed. Fig. 7 compares these five flow patterns with the observed flow patterns on the heated surface.
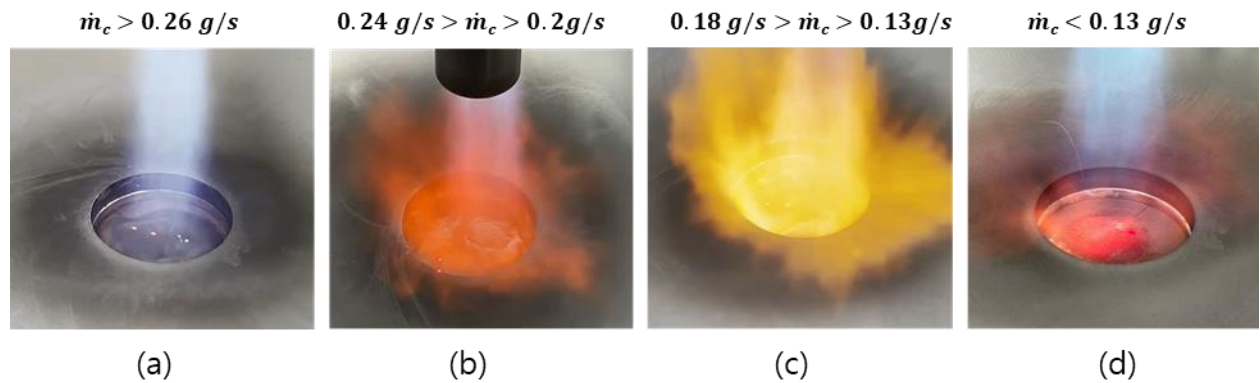

Fig. 7 Images of (a) all liquid region, (b) liquid-mixture region, (c) liquid-mixture-vapor and mixture-vapor region, and (d) all vapor region flow patterns according to coolant mass flow rate, respectively.

As represented in Fig. 7 (a), when the range of coolant mass flow rate is greater than 0.26 g/s, the coolant is discharged onto the heated surface in the liquid state, forming a liquid film. This range corresponds to the pattern (1) among the five flow patterns, characterized by "All liquid," where an overcooling phenomenon, solely through single-phase heat transfer, is observed, capable of removing the given heat flux. As depicted in Fig. 7 (b), when the range of cooling water mass flow rate was between 0.2 and 0.26 g/s, bubbles were observed forming and escaping due to phase change on the heated surface of the porous specimen. As the coolant flow rate decreases, a more rapid cycle of bubble formation and release is observed across the entire heated surface area. This range corresponds to the pattern (2), where phase change begins from the heated surface, leading to the appearance of a liquid-mixture interface. Fig. 7 (c) corresponds to the range of coolant mass flow rate between 0.13 and 0.18 g/s. Here, it was observed that the phase change region penetrates deeper from the heated surface of the porous specimen, with no further bubble formation observed on the surface. Instead, an internal phase change occurs, leading to vapor discharge. This range corresponds to patterns (3) and (4), where the liquid-mixture interface descends as the coolant flow rate decreases, transitioning from pattern (3) to pattern (4), where the liquid phase disappears. This can be confirmed through the temperature of the fluid at the bottom of the specimen, as will be discussed more specifically in the following section. As represented in Fig. 7 (d), when the range of cooling water mass flow rate is less than 0.13 g/s, dry-out occurs throughout the entire porous media. In this case, proper cooling does not occur, resulting in continuous temperature rise of the specimen, ultimately leading to its destruction. This range corresponds to the pattern (5), characterized by the Dry-out region where only the overheated vapor region exists throughout the porous media.
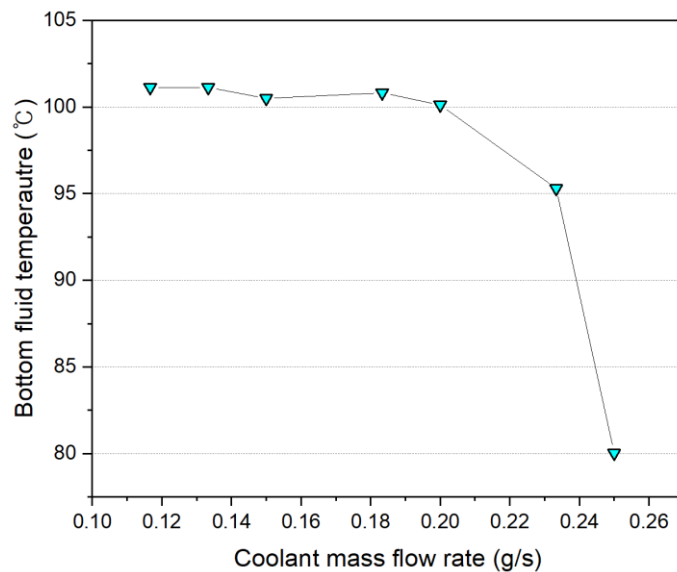
3.1.3 Pressure drop and heat transfer

As illustrated in Fig. 8, Pressure measurements obtained in the coolant chamber exhibit an "N" shaped pressure curve corresponding to changes in coolant mass flow rate. These pressure changes are closely associated with the five observed flow patterns discussed in Section 3.3.
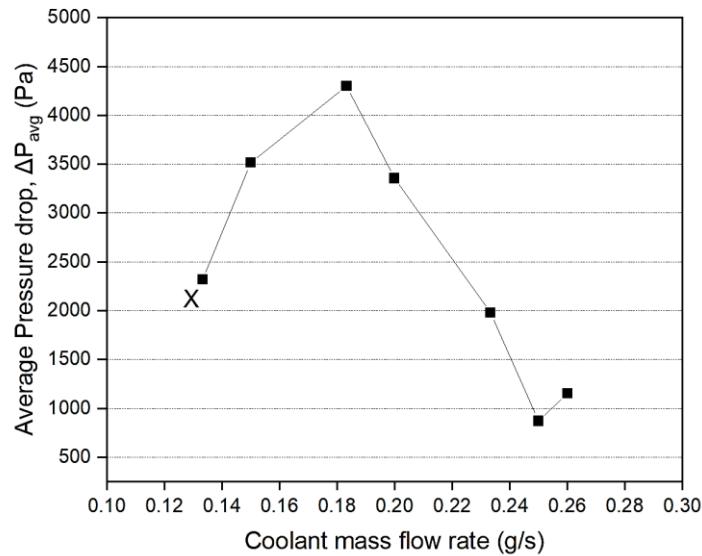
Fig. 8 Pressure drop result

As the coolant mass flow rate decreases, there is a decrease in pressure within the all-liquid region due to the reduced velocity of the single-phase coolant. Subsequently, in the regime corresponding to the pattern (2), pressure rises again due to vapor generation from phase change, leading to the expansion of these vapors hindering fluid flow. With further reduction in coolant flow, the mixture region thickens, resulting in increased pressure. In the (3, 4) regimes, as coolant diminishes further, the phase change region penetrates deeper into the porous medium. Additionally, the coolant flow rate is slow, which shortens the length of the phase change region and thus reduces pressure. At this stage, vapor blocking and flow instability phenomena were observed where vapor trapped in the pores grows to the pore size and impedes the flow until they are periodically released with liquid expulsion. As coolant was further reduced, changes in the frequency and timing of liquid discharge were observed. In the all-vapor region, continuous temperature rise led to specimen thermal destruction, with no recorded pressure measurements.

Fig. 9 Temperature result

The Effect of Sintering Condition on the Properties and Transpiration Cooling Performance of Porous Ni-based Superalloy

This mass flow rate-pressure graph has similar characteristics to forced convection boiling in a microchannel. Therefore, the heat transfer characteristics were analyzed by comparing the five flow patterns observed in this study with the five flow patterns that appear in forced convection boiling within the microchannel: all vapor, saturated boiling, low superheated subcooled boiling, high superheated subcooled boiling, and all liquid.

Fig. 9 represents the fluid temperature at the bottom of the specimen, and it was confirmed that the temperature changed according to five flow patterns. As the coolant decreases in the all-liquid section, the convective heat transfer coefficient decreases, causing the temperature to increase rapidly. In the high superheated subcooled boiling section, the phase change begins from the top of the specimen, and the temperature measured at the bottom gradually increases below the phase change temperature. A decrease can be seen in the low superheated subcooled boiling section, which is because the phase change inside the specimen becomes more active and the convective heat transfer coefficient increases. Next, in the saturated boiling section, the bottom temperature becomes the phase change temperature and is maintained, and the temperature increases again in the all-vapor region.

Conclusions

In this study, porous metal specimens were fabricated using powder sintering with Hastelloy X powder. The physical characteristics of the specimens were analyzed based on the compaction pressure and sintering temperature in the manufacturing process. The process variables for producing specimens with the target porosity of 0.3 were determined, which included a compaction pressure of 19.5 MPa and a sintering temperature of 1100 °C. Using these established process variables, three specimens with different porosities were created. Subsequently, the radiative cooling performance was analyzed under heat flux conditions ranging from 0.5 to 2.0 MW/m2 and a cooling water injection rate of 1 g/s.

Acknowledgements

References

1. Borrelli, Rosario, et al. "Thermo-structural behaviour of an UHTC made nose cap of a reentry vehicle." *Acta Astronautica* 65.3-4 (2009): 442-456.

2. Pulci, Giovanni, et al. "High temperature mechanical behavior of UHTC coatings for thermal protection of re-entry vehicles." *Journal of thermal spray technology* 20 (2011): 139-144.

3. Abdi, Frank, et al. "Collision provoked failure sequencing in space reentry vehicles." *Computers & structures* 89.11-12 (2011): 930-939.

4. Viviani, Antonio, et al. "Aeroshape design of reusable re-entry vehicles by multidisciplinary optimization and computational fluid dynamics." *Aerospace Science and Technology* 105 (2020): 106029.

5. Yinhai, Z. H. U., et al. "Review on active thermal protection and its heat transfer for airbreathing hypersonic vehicles." *Chinese Journal of Aeronautics* 31.10 (2018): 1929-1953.

6. van Foreest, Arnold, et al. "Transpiration cooling using liquid water." *Journal of Thermophysics and Heat Transfer* 23.4 (2009): 693-702.

7. Langener, Tobias, et al. "Experimental investigations of transpiration cooling applied to C/C material." *International Journal of Thermal Sciences* 54 (2012): 70-81.

8. Langener, Tobias, Jens Von Wolfersdorf, and Johan Steelant. "Experimental investigations on transpiration cooling for scramjet applications using different coolants." *AIAA journal* 49.7 (2011): 1409-1419.

The Effect of Sintering Condition on the Properties and Transpiration Cooling Performance of Porous Ni-based Superalloy